

Demonstration of Package Level 3D-printed Direct Jet Impingement Cooling applied to High power, Large Die Applications

T.-W. Wei^{1,2}, H. Oprins¹, V. Cherman¹, Z. Yang³, K. Rivera^{3*}, G. Van der Plas¹,
B. J. Pawlak⁴, L. England³, E. Beyne¹ and M. Baelmans²

¹IMEC, Leuven, Belgium, ²Dept. Mech. Eng. KU Leuven, Leuven, Belgium, ³GlobalFoundries, Malta, NY, US,

⁴GlobalFoundries at IMEC, Leuven, Belgium

Email: tiwei.wei@imec.be

Abstract—This work presents, for the first time, a package-level, bare die liquid jet impingement 3D polymer microfluidics heatsink fabricated using 3D printing, or additive manufacturing for large die size and high-power applications. The heatsink achieves a chip temperature increase of 17.5°C at a chip power of 285 W for a coolant flow rate of 3.25 LPM, demonstrating that 3D printing enables the design for low-cost, high efficiency direct on-chip microfluidic heatsink with complex internal 3D manifold liquid delivery channels. The measurement results show that the jet impingement cooling performance can be successfully described using a unit cell approach, allowing an easy scaling of the thermal performance for arbitrary die size applications. Long term thermal tests of 1000h show a constant thermal performance and no degradation of the cooler material.

Index Terms—Liquid cooling, power electronics, jet impingement cooling, low cost fabrication, high power

I. INTRODUCTION

With the increasing demand on the functionality and higher computation performance for high performance chips, the die size is continuously increasing. For example, the die size has increased from 12 mm² in 1971 to 688 mm² in 2019 for Intel microprocessors, and from 270 mm² in 1998 to 696 mm² in 2019 for IBM microprocessors [1]. Moreover, the chip power also increases with the increase of performance, especially for the emerging applications, such as machine learning or artificial intelligence (AI) computing, high performance computing (HPC) and networking applications [1,2].

For the traditional microchannel cooling applied in the large die size and high power applications, the temperature gradient along the chip area will be a concern. Advanced micro/nanofluidic cooling techniques, such as interlayer cooling [3] and intra-die cooling [4] have been proposed and demonstrated, showing high cooling performance. These solutions are however not compatible with the fine pitch requirements for high bandwidth communication between different tiers of a 3D system. Microscale jet impingement cooling on the bare die is an efficient cooling technique where the liquid coolant is directly ejected on the chip backside, as shown in Fig.1. This microfluidic cooling system contains a high density of local level microjet nozzles and global level fluidic delivery manifold microchannels. This concept has been successfully applied with silicon processing [5], multilayer ceramic technology [6] and mechanical micromachining [7, 8]. However, these methods require the different individual parts to be fabricated separately and then assembled together. Moreover, it is also shown that the geometry of the manifold in microfluidic heatsinks has a dominant impact on the system pressure drop and thermal performance [9]. This impact will be

even more pronounced for large die size applications due to the coolant flow non-uniformity over the chip surface.

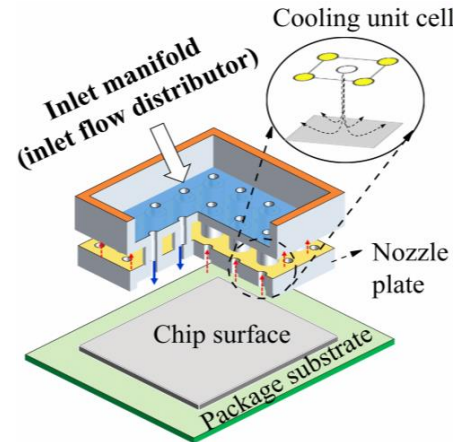


Figure 1: Schematic concept of the package level 3D microfluidic heatsink with microscale inlet/outlet nozzles and 3D manifold liquid delivery systems.

Additive manufacturing, or 3D printing, is regarded as a promising technique for on-demand electronics manufacturing [10] and for the fabrication of complex geometries in various materials, which can provide more design flexibility for the complex internal geometry of microfluidic coolers. In our previous studies [11, 12], we presented package-level 3D printed jet impingement coolers demonstrated for single 8×8 mm² test chips and for 2.5D interposer package with two test chips, shown in Fig.2, and for targeted hot spot cooling [13, 14]. The experimental and numerical [15] studies prove that the nozzle array cooling is area independent for a constant nozzle flow rate by normalizing all the parameters: thermal resistance, flow rate and pressure drop. Therefore, the cooling performance of the large die size cooler can be extrapolated from the characterized results of 3D printed cooler demonstrated before.

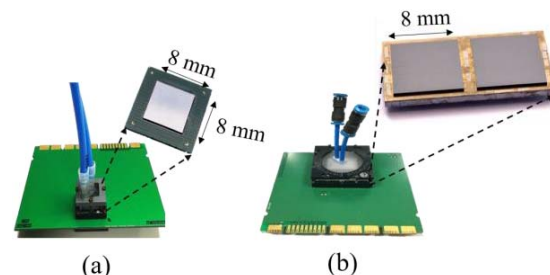


Figure 2: Demonstration of the single die cooler [10] and interposer package cooler [11] with two thermal test dies.

In this paper, the liquid jet impingement cooling concept with a scalable nozzle array is applied to the large die size applications, for a die sizes above 500 mm², and for high power applications (>250W). The objective is to provide a proof of concept that this cooling solution, that was previously demonstrated on the small die size of the test chip, can be scaled-up to relevant chip sizes and power dissipation values. We discuss the design, fabrication, and experimental characterization of the 3D printed large-die cooler and the assessment of the cooler performance over a 1000h long period of operation.

II. 3D PRINTED MICROFLUIDIC HEATSINK

A. Large die size thermal test vehicle

In order to characterize the thermal performance of the 3D printed microfluidic heatsink, a 23×23 mm² thermal test chip, shown in Fig.3 is used. This passive test chip contains 16 heater zones and 25 temperature sensors as metal meanders in the BEOL. The calibrated temperature coefficient of the resistance is 3553±2 ppm/°C in the temperature range of 10°-70°C. The heaters generate a power of 250-285W (depending on the chip temperature) for an applied voltage of 50V. The test chip is flip-chip mounted on a package laminate substrate of 55×55 mm². The thermal performance of the microfluidic cooler is evaluated both on a lidded package (1 mm thick Cu lid) as well as on a bare die package with an exposed chip backside accessible for direct liquid cooling.

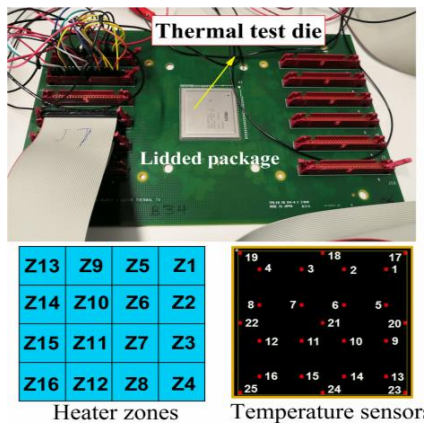


Figure 3: 23 mm × 23 mm thermal test chip with 16 heater zones and 25 temperature sensors. The 55×55 mm² package is assembled to the test board (lidded package version shown).

B. Large die cooler design

The main design considerations for the large die cooler are the inlet flow uniformity and the possible die and package warpage of the large die assembly. The microfluidic heatsink configuration matching the dimensions of the chip package is shown in Fig.4, with a nozzle array below the coolant entrance connection. The jet nozzle plate in Fig. 4, contains an 11×11 inlet jet array and a 12×12 array of outlets distributed in between the inlets, with a nozzle pitch of 2 mm and a nozzle diameter of 600 μm. The nozzle geometry is the same as for the single die coolers [10, 11], only the number of nozzles has been scaled to match the die area. The cavity height, defined as the

nozzle-to-chip surface distance is 600 μm. The total cooler size is 55×55×17.5 mm³. To accommodate the package warpage, O-rings are used, for which a dedicated groove is foreseen in the cooler design. Table 1 lists the critical dimensions' comparison with the single die cooler, interposer cooler and the large die cooler.

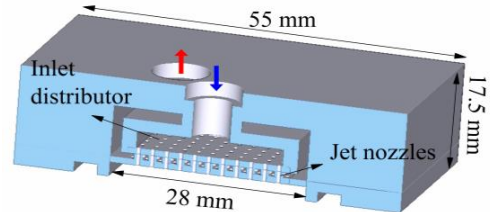


Figure 4: Cross-section view of the microfluidic cooler configurations with nozzle array below coolant entrance connection.

Table 1: Scaling from single die cooler to large die cooler

Geometry		Single cooler [11]	Interposer cooler [12]	Large die cooler
Nozzle array	N	4×4	4×4 per die	11×11
Nozzle pitch		2 mm	2 mm	2 mm
Inlet chamber		2.5 mm	2.5 mm	3 mm
Inlet diameter	d_i	0.6 mm	0.6 mm	0.6 mm
Outlet diameter	d_o	0.6 mm	0.6 mm	0.6 mm
Cavity height	H	0.6 mm	0.6 mm	0.6 mm
Nozzle plate thickness	t	0.55 mm	0.55 mm	0.55 mm
Cooler size	x,y,z	14×14×8.7 (mm ³)	35×35×9.1 (mm ³)	55×55×17.5 (mm ³)

C. Large die cooler fabrication

The microfluidic heatsinks (Fig. 5) are fabricated using high resolution Stereolithography (SLA) 3D printing with a minimal feature size of 70 μm, using the water-resistant material Sonos WaterShed XC 11122 [11,12,16]. The side view of the transparent coolers in Fig. 5 reveals the successfully fabricated internal structures of the cooler design, that could not be fabricated with conventional fabrication techniques. The fabrication tolerance of the fabricated nozzles is assessed using 2D and reconstructed 3D microscope images (Fig. 6). The measured average nozzle diameter is 630 μm, which deviates only 5% from the nominal design value of 600 μm. Moreover, a full array of nozzles from the bottom view of the large die cooler is shown in Fig.7. This demonstrates that additive manufacturing can be used for the fabrication of complex microfluidic cooler geometries with micro-scale features.

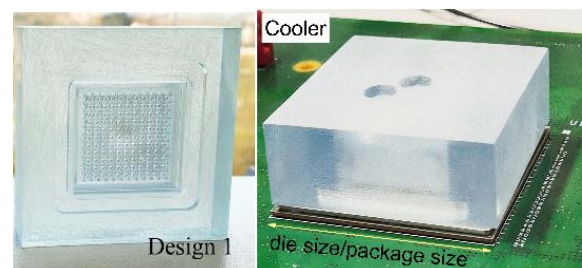


Figure 5: Images of the demonstrated cooler: the cooler size is matched to the large die/package size.

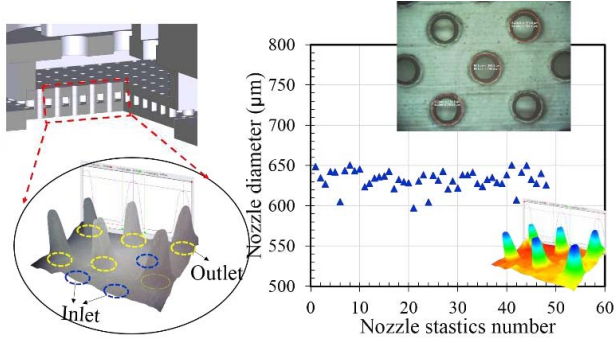


Figure 6: Nozzle geometry and nozzle diameter evaluation with 2D and reconstructed 3D microscope image: 5% deviation from the nominal design value of 600 μm .

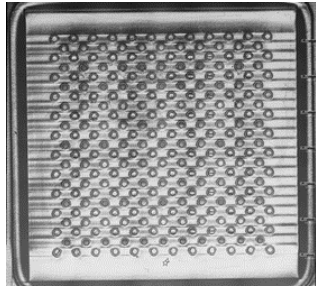


Figure 7: Microscope image of the cooler bottom showing the inlet and outlet nozzle array.

III. EXPERIMENTAL CHARACTERIZATION

A. Large die cooler setup and calibration

For the thermal and hydraulic characterization of the large die coolers, the 3D printed coolers are connected to the closed-loop fluidic circuit. The details of the fluidic and electrical connections to the large die test chip are shown in Figure 8(a). Moreover, the schematic of the electrical control for the heaters in the large die is shown in Figure 8(b). In general, all the heaters connected to single power supply, with 4 parallel chains of 4 heaters in series to dissipate uniform power. Off-chip resistors are designed to measure the current in each branch.

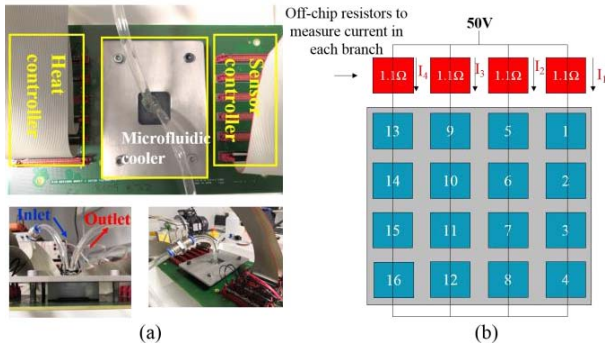


Figure 8: Measurements set-up: (a) Details of the fluidic and electrical connections to the test vehicle in the flow loop; (b) schematic of the 16 heaters in the large die.

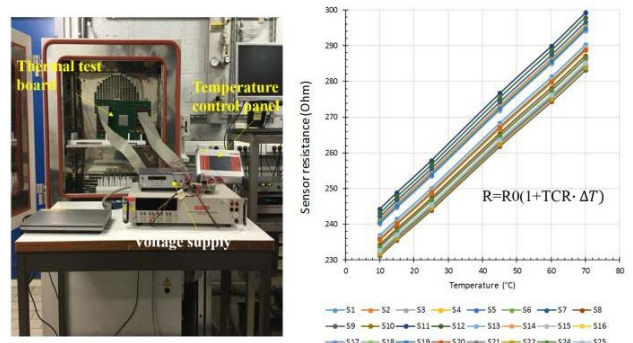


Figure 9: Calibration of the TSRs in the large die thermal test vehicle: (a) TSR calibration setup; (b) Sensor resistance as function of temperature for 25 sensors.

In the second step, the 25 temperature-sensitive resistors (TSR) are calibrated as a function of temperature [8]. The experimental setup and the sensor resistance as function of the temperature are illustrated in Figure 9. The range of the calibrated temperature is from 10°C to 70°C. The calibrated TCR is $3553 \pm 2 \text{ ppm}/^\circ\text{C}$. Therefore, the temperature increase of the sensor ΔT can be determined by the following equation [17]:

$$\Delta T = \frac{R - R_0}{R_0 \cdot \text{TCR}} \quad (1)$$

where R_0 is the resistance at the reference temperature. The TCR is the temperature coefficient of the resistance.

B. Characterization of the heatsink

The distribution of the measured chip temperature increase with respect to the coolant inlet temperature in the bare die package for a chip power of 275W and a coolant (DI water) flow rate of 3.25 LPM is shown in Fig.10(a). At this power, an average chip temperature increase as low as 17.5°C is achieved with a low temperature non-uniformity of 6% for a low pressure drop of 0.7 bar, demonstrating the efficiency of the microfluidic cooler. Fig.10(b) shows the measured chip temperature profile along the chip diagonal for three different flow rates for a total applied voltage of 50V. The average temperature increase is defined as the average chip temperature with respect to the coolant inlet temperature.

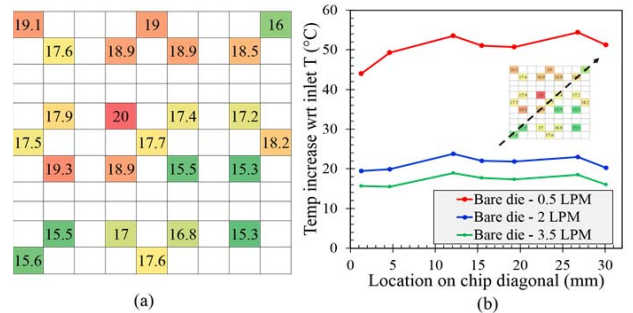


Figure 10: Temperature measurement on the test chip for a total applied voltage of 50V using the large die cooler: (a) Temperature distribution map for a constant flow rate of 3.25 LPM; (b) Temperature profile along the large die diagonal with total applied voltage of 50V.

The evolution of the average temperature increase as a function of the chip power for constant flow rate of 1 L/min is plotted in Fig.11(a). The thermal resistance can be extracted from the correlation between the measured chip temperature increase and the applied chip power. The average thermal resistance for a coolant flow rate of 1 LPM is 0.14 K/W. Moreover, the evolution of the average chip temperature increase as a function of the flow rate for a total applied voltage of 50V is plotted in Fig.11(b). The temperature increase as a function of flow rate shows as a power law relation, with an exponent of -0.55. The normalized thermal resistance comparison in Fig.12 shows that the scaled large die cooler has the same normalized thermal performance as the 4x4 array cooler on the 8x8 mm² PTCQ [12, 18]. Therefore, the implementation of the multi-jet cooling on the large die size with the 11x11 nozzle array validates the scalability of this unit cell based cooling concept. The thermal performance of the cooling on this 530 mm² die can be extrapolated to cooling power of 1kW for a maximum chip temperature increase of 65°C for a flow rate of 27 ml/min per nozzle or 3.25LPM for the total cooler.

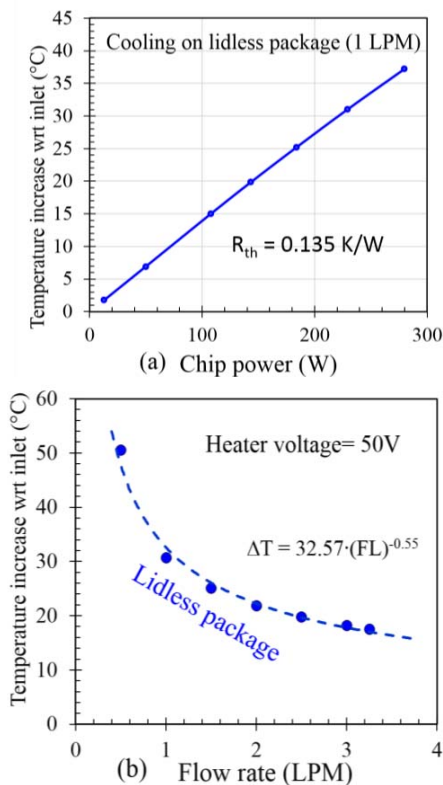


Figure 11: Temperature measurements of the cooling on the bare die package at (a) different chip power values and (b) different flow rates at total heater voltage of 50V.

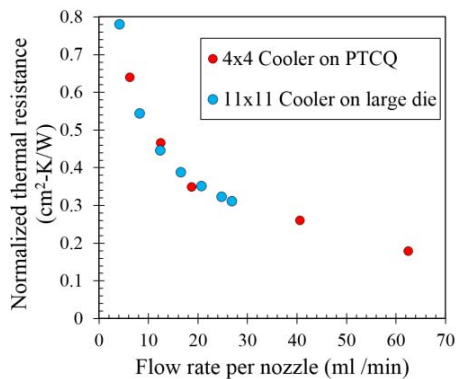


Figure 12: Scaled large die cooler shows the same thermal performance as the 4x4 array cooler on the 8x8 mm² PTCQ with the same nozzle geometry in terms of the normalized thermal resistance.

C. Comparison cooling on lidded package vs bare die

For the 2.5D interposer package shown in [12], the thermal conductivity of the TIM is 1.9 W/m-K and the bond line thickness is 90 μm, as illustrated in Table 2. This results in a large difference between the bare die and lidded package cooler of a factor of 2.5 to 3. For this test vehicle, the thermal conductivity of the TIM is 2.3 W/m-K with a thickness of 20 μm. Therefore, the difference between the bare die package and lidded package cooling is expected to be smaller for this large die package.

Table 2: Comparison of the TIM material parameters

TIM	Interposer package [12]	Large die package
TIM thickness	90 μm	20 μm
TIM conductivity	1.9 W/m-K	2.3 W/m-K

The measured temperature distribution profiles for the lidded package and the lidless package for different flow rate values and for a total applied voltage of 50V are shown in Fig.13. The average chip temperature increase and the measured coolant temperature increase are shown in Fig.14 as a function of the flow rate.

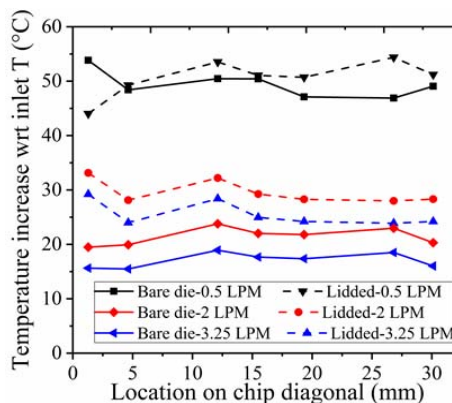


Figure 13: Temperature increase with respect to the inlet temperature comparison with the lidded and bare die package

for a total applied voltage of 50V: temperature profile comparison on the chip diagonal.

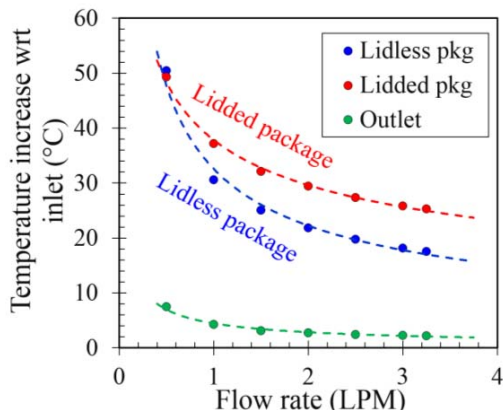


Figure 14: Temperature increase with respect to the inlet temperature comparison with the lidded and bare die package for a total applied voltage of 50V: averaged temperature comparison as function of the coolant flow rate.

The measurements show that the cooling on the lidded package has a slightly better thermal performance at very low flow rates, due to the lateral thermal spreading in the metal lid, while the bare die cooling outperforms the cooling on the lid for flow rate values above 0.7 LPM. This is because increasing the cooling rate, reduces the relative contribution of the heat spreading in the lid. At a flow rate of 2 LPM, the temperature increase of the cooler on the bare die package is 35% lower compared to the lidded package. For a higher flow rate of 3.25 LPM, the temperature difference is increased to 44%. This is caused by the additional thermal resistance of the lid and mainly the thermal interface material in the thermal path between the heat source and the cooling solution, in case of the lidded package. The temperature difference between the bare die cooling and lidded package cooling is summarized in Fig. 15. It can be seen that the temperature difference becomes larger with the increase of the flow rate.

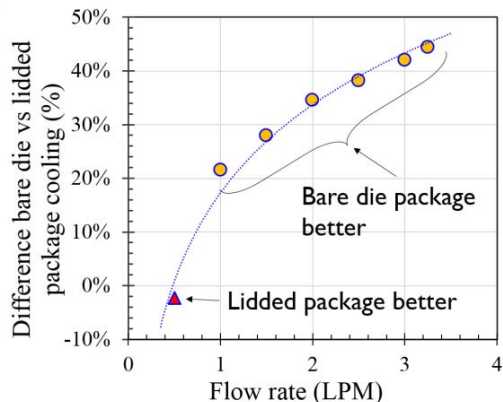


Figure 15: Temperature difference between the bare die cooling compared with the lidded package cooling.

For the comparison of the bare die package and lidded package cooling, the chip temperature uniformity is also investigated, as illustrated in Fig. 16. The bare die cooling shows 8.1% temperature variation over the die area while the

lidded package shows 6.4% variation at a flow rate of 1 LPM. The difference between the maximum chip temperature and minimum chip temperature is also compared as shown in Fig. 17. It can be seen that this temperature difference is 16% lower for the bare die cooling at a flow rate of 3.25 L/min. In general, for the bare die cooling at a flow rate of 3.25 L/min, it shows about 45% lower thermal resistance, and 16% lower temperature gradient compared to the cooling on the lidded package. Therefore, bare die cooling without lid (and TIM) shows better cooling performance than the lidded package. However, lidless cooling is considered as less reliable and therefore more challenging to maintain than cooling on the lid. Therefore, in the following part, the long-term performance of the bare die cooling is experimentally evaluated.

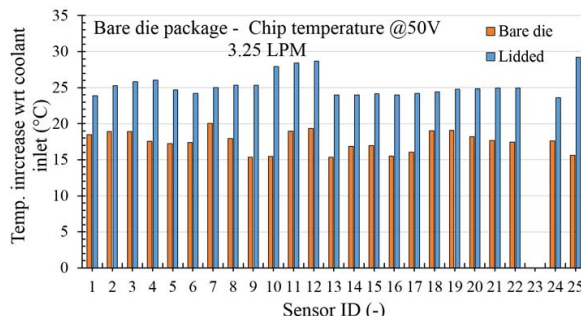


Figure 16: Temperature increase variations for different temperature sensors at a flow rate of 3.25 LPM for a total heater voltage of 50V.

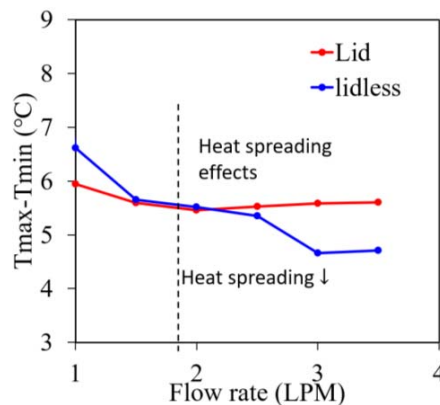


Figure 17: Maximal temperature difference over the chip area as function of the flow rate for bare die cooling and lidded package cooling.

IV. LONG TERM COOLING MEASUREMENT

A. Long-term cooling measurements

For direct on-chip liquid cooling, there are several concerns such as the cooling performance over time and potential reliability issues of the devices. In order to evaluate these aspects of the 3D printed microfluidic cooler, a longer-term measurement of the cooler is being conducted during 50 days in a closed loop system with DI water as coolant, where the chip temperature and ambient temperature are monitored. The cooler geometry and nozzle diameter are inspected before and after the

long-term measurements. In order to perform the long-term measurement for the large die liquid cooling, a simplified set-up with an integrated pump and heat exchanger is developed for the thermal and flow measurement, shown in Fig. 18. Temperature measurements are performed in all 25 sensors of the test chip during the long-term measurement. The test board is placed in the plastic tray to check for potential leakages that might occur during the test.

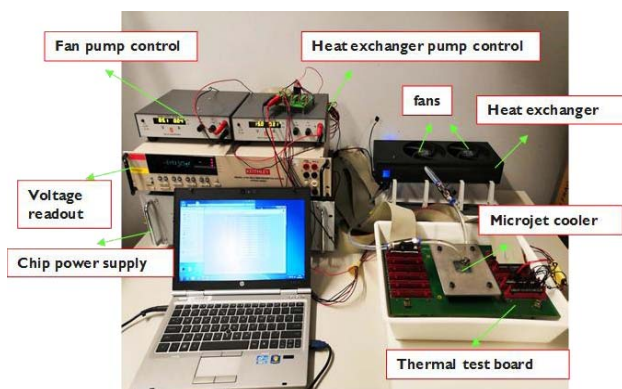


Figure 18: Simplified set-up developed for thermal and flow measurement.

For the test conditions, the measured actual power in the heaters of the test chip is 90 W for an applied voltage of 30V. The pump voltage is 12V and the heat exchanger voltage is 10 V. Since the flow rate is controlled by the pump voltage, the flow rate in this experiment is estimated by the thermal performance, which is estimated as 1.5 L/min based on the performance reported in Fig. 14.

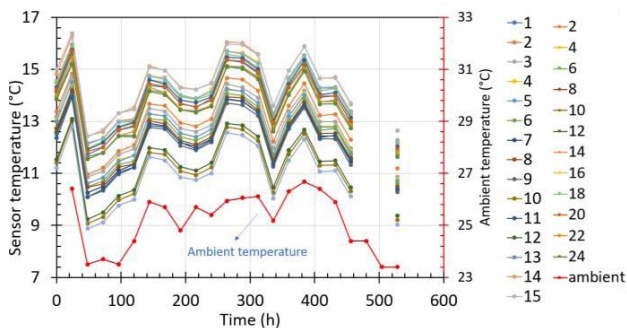


Figure 19: Trend for all temperature sensors and the ambient temperature during the long-term measurements, compared with the ambient temperature.

During the long-term measurement, the ambient temperature is also monitored as shown in Fig.19. It can be seen that the trend of the absolute temperature for all the sensors is consistent with the trend of the ambient temperature. Therefore, the reported temperature increase is defined as the average chip temperature with respect to the ambient temperature. Fig. 20 shows that the thermal performance of the 3D printed large die cooler remains constant over the measurement period of 1000 hours. During this period, no reliability issues have been observed.

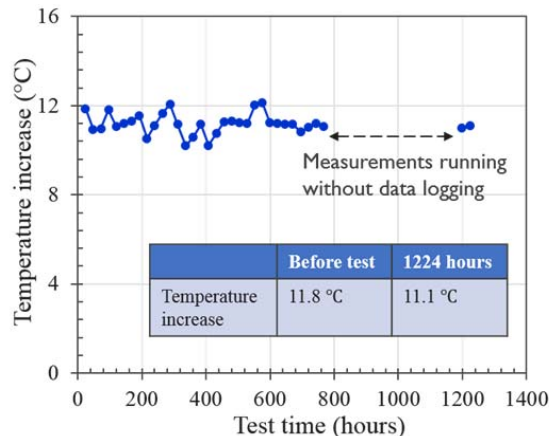


Figure 20: Long term temperature measurement (50 days): Evolution of the average chip temperature increase with respect to the actual ambient temperature.

B. Cooler geometry impact

In order to evaluate the nozzle diameter variation before and after the long-term measurement, the nozzle diameter is measured. From the cross-section analysis in Fig.21, no clogging of the nozzles or internal channels is observed despite the lack of filters in the simple test setup. Also, no erosion of the nozzles is observed. In addition, there is no significant difference for the nozzle diameters before and after the measurements, as show in Fig.22.

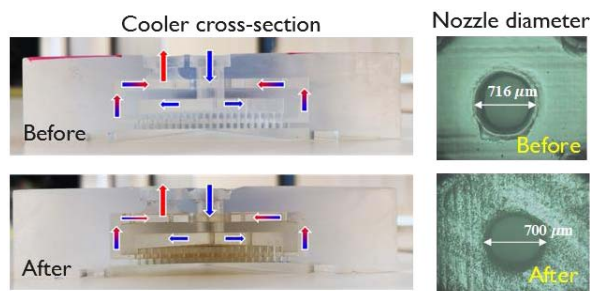


Figure 21: Cross section analysis after long term measurement with DI water for the 3D printed plastic cooler.

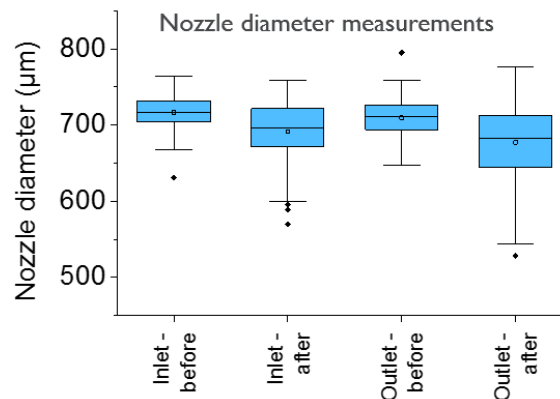


Figure 22: No significant difference for the nozzle diameters before and after the measurements.

V. BENCHMARKING WITH STANDARD AIR COOLING

Fig.23 shows the performance benchmarking of the measurement data of the present work with a reference air cooling solution consisting of a heat sink and fan for a power of 90 W dissipated in the test vehicle. The comparison is reported for the chip temperature increase with respect to the ambient, which is the air temperature in case of air cooling and the coolant inlet temperature in case of the microfluidic cooling. The benchmarking study shows that this package level 3D microfluidic heatsink can achieve a chip temperature reduction with factor of 4 and 5 for the cooling on the lidded package and bare die package respectively compared to the standard air-cooling. In addition, Fig.24 illustrates the drastic size and weight reduction of the cooler from the bulky heat sink-fan combination to the cooler that matches the package size allowing a higher package density.

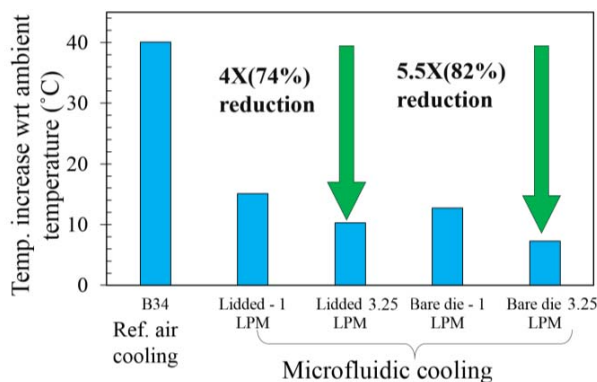


Figure 23: Cooler benchmarking for 90W chip power: the 3D printed microfluidic heatsink on the bare chip improves the cooling performance by a factor of 5 compared to a standard air-cooled heat sink.

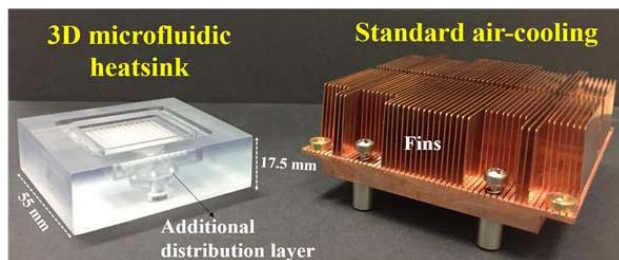


Figure 24: Benchmarking study: size comparison of the standard air-cooling solution and the package-size impingement cooling solution.

VI. CONCLUSIONS

In this paper, we demonstrated for the first time the fabrication and characterization of a package-level 3D polymer jet impingement cooler with impingement jets fabricated using 3D printing, applied to a 23×23 mm² large die with 285W power dissipation. For a coolant (DI water) flow rate of 3.25 LPM, the average chip temperature increase is as low as 17.5°C with a pressure drop of 0.7 bar. Extrapolated to an allowable chip temperature increase of 60°C, this results in a

cooling power of 1kW over the die area of 23×23 mm². At the flow rate of 3.25 LPM, the cooling on the bare die package outperforms the cooling on the lidded package by 44% and results in a reduction of the temperature gradient by 16%.

The benchmarking study shows that the 3D printed microfluidic heatsink improves the cooling performance by a factor of 5 combined with a large reduction in cooler size and weight, compared to a standard air-cooled heat sink. Moreover, it is demonstrated that additive manufacturing enables the accurate fabrication of complex internal structures in multiple layers inside the microfluidic heatsink as one single piece. A longer-term measurement of 1000h of the cooler has been conducted in a closed-loop liquid coolant system with DI water, where the chip temperature and ambient temperature were monitored. The cooler geometry and nozzle diameters are inspected before and after the long-term measurements. The measurements show that the thermal performance of the microfluidic cooler remains constant over the measurement period of 1000 hours. During this period, no reliability issues have been observed.

ACKNOWLEDGMENT

This work was performed as part of the imec Industrial Affiliation Program on 3D System Integration and has been strongly supported by the imec partners.

REFERENCES

- [1] El-Aawar, Haissam. "Increasing the transistor count by constructing a two-layer crystal square on a single chip." *International Journal of Computer Science & Information Technology (IJCSIT)* 7.3 (2015): 97-105.
- [2] Joel Hruska, "Intel Details Its Nervana Inference and Training AI Cards", <https://www.extremetech.com/computing/296990-intel-nervana-nnp-i-ann-t-a-training-inference>, August 21, 2019.
- [3] Brunswiler, Thomas, et al. "Towards cube-sized compute nodes: Advanced packaging concepts enabling extreme 3D integration." 2017 IEEE International Electron Devices Meeting (IEDM). IEEE, 2017.
- [4] Dang, B., Joseph, P. J., Wei, X., et al., "A Chip-Scale Cooling Scheme With Integrated Heat Sink and Thermal-Fluidic I/O Interconnects". In *ASME 2005 Pacific Rim Technical Conference and Exhibition on Integration and Packaging of MEMS, NEMS, and Electronic Systems* collocated with the ASME 2005 Heat Transfer Summer Conference (2005): 605-610.
- [5] Brunswiler, Thomas, et al. "Interlayer cooling potential in vertically integrated packages." *Microsystem Technologies* 15.1 (2009): 57-74.
- [6] Natarajan, Govindarajan, and R. J. Bezama. "Microjet cooler with distributed returns." *Heat transfer engineering* 28.8-9 (2007): 779-787.
- [7] Tiwei, T., Herman Oprins, et al., "High efficiency direct liquid jet impingement cooling of high power devices using a 3D-shaped polymer cooler." In *2017 IEEE International Electron Devices Meeting (IEDM)*, pp. 32-5. IEEE, 2017.
- [8] Wei, T-W., et al. "Experimental characterization and model validation of liquid jet impingement cooling using a high spatial

resolution and programmable thermal test chip." *Applied thermal engineering* 152 (2019): 308-318.

[9] Ryu, J. H., Do Hyung Choi, and SungJin Kim. "Three-dimensional numerical optimization of a manifold microchannel heat sink." *International journal of heat and mass transfer* 46.9 (2003): 1553-1562.

[10] Veres, J., R. D. Bringans, E. M. Chow, J. P. Lu, P. Mei, S. E. Ready, D. E. Schwartz, and R. A. Street. "Additive manufacturing for electronics "Beyond Moore"." In 2016 IEEE International Electron Devices Meeting (IEDM), pp. 25-6. IEEE, 2016.

[11] Wei, T. W., et al., "Experimental Characterization of a Chip-Level 3-D Printed Microjet Liquid Impingement Cooler for High-Performance Systems." *IEEE Transactions on Components, Packaging and Manufacturing Technology* 9.9 (2019): 1815-1824.

[12] Wei, T. W., et al., "Experimental and numerical investigation of direct liquid jet impinging cooling using 3D printed manifolds on lidded and lidless packages for 2.5 D integrated systems." *Applied Thermal Engineering* 164 (2020): 114535.

[13] Wei, Tiwei, et al. "Low-cost Energy Efficient On-chip Hotspot Targeted Microjet Cooling for High Power

Electronics." *IEEE Transactions on Components, Packaging and Manufacturing Technology* (2019).

[14] Wei, Tiwei, Herman Oprins, Vladimir Cherman, Ingrid De Wolf, Eric Beyne, and Martine Baelmans. "First Demonstration of a Low Cost/Customizable Chip Level 3D Printed Microjet Hotspot-Targeted Cooler for High Power Applications." In 2019 IEEE 69th Electronic Components and Technology Conference (ECTC), pp. 126-134. IEEE, 2019.

[15] Wei, Tiwei, et al. "Conjugate Heat Transfer and Fluid Flow Modeling for Liquid Microjet Impingement Cooling with Alternating Feeding and Draining Channels." *Fluids* 4.3 (2019): 145.

[16] Fei, Guanghai; Wei, Tiwei; 2019. Preliminary Study on Hybrid Manufacturing of the Electronic-Mechanical Integrated Systems (EMIS) via the LCD Stereolithography Technology. The 30th Annual International Solid Freeform Fabrication Symposium - An Additive Manufacturing Conference.

[17] W. Bolton, "2.7.3 Resistance temperature detectors (RTDs)", in *Instrumentation and Control Systems*, 2004.

[18] Oprins, H., Cherman, V., Van der Plas, G., De Vos, J. and Beyne, E., "Experimental characterization of the vertical and lateral heat transfer in three-dimensional stacked die packages. *Journal of Electronic Packaging*", 2016, 138(1).